Study of MBBR-MBR Performance by the Addition of Commercial and 3D-Printed Biocarriers

Dimitra C. Banti *, Petros Samaras, Eleni Kostopoulou, Vassiliki Tsioni, Themistoklis Sfetsas

Posted Date: 6 June 2023

doi: 10.20944/preprints202306.0393.v1

Keywords: MBBR-MBR; biofilm; 3D-printed biocarriers; Kaldnes K1 biocarriers; 13X-halloysite biocarriers; membrane fouling; SMP; EPS; colloidal particles; wastewater treatment

Article

Study of MBBR-MBR Performance by the Addition of Commercial and 3D-Printed Biocarriers

Dimitra C. Banti [1,2,*], Petros Samaras [2], Eleni Kostopoulou [1], Vassiliki Tsioni [1] and Themistoklis Sfetsas [1]

[1] QLAB Private Company, Research & Development, Quality Control and Testing Services, 57008 Thessaloniki, Greece; e.kostopoulou@q-lab.gr; vtsioni@q-lab.gr; tsfetsas@q-lab.gr

[2] Department of Food Science and Technology, School of Geotechnical Sciences, International Hellenic University, GR-57400 Thessaloniki, Greece; samaras@ihu.gr

* Correspondence: bantidim@gmail.com (D.B.); Tel.: +30-2310013903

Abstract: For this research, a comparative evaluation was performed in which the addition of 3D-printed biocarriers fabricated with 13X and Halloysite (13X-H) and commercial Kaldnes K1 biocarriers were evaluated as opposed to the non addition of biocarriers in a semi-pilot scale MBBR-MBR unit. For the evaluation of the MBBR-MBR efficiency, various physicochemical parameters were measured while static light scattering and optical microscopy observations were additionally used. Biofilm extracted from the biocarriers was also evaluated. It was observed that in the MBBR-MBR K1 unit, the membrane filtration improved while in the MBBR-MBR 13X-H unit the membrane fouling rate was the same as in the control MBBR-MBR unit. This is due to the production of large amount of SMP which resulted from the large amount of biofilm created in the 13X-H biocarriers. An optimal biodegradation of the organic load was concluded for all three MBBR-MBR units. The nitrification and denitrification processes were improved at the MBBR-MBR units using 13X-H and K1. The dry mass produced on the 13X-H biocarriers was three orders of magnitude larger than that produced on the K1. Finally, it was observed that mostly EPS was produced in the biofilm of K1 biocarriers while in the biofilm of 13X-H mostly SMP.

Keywords: MBBR-MBR; biofilm; 3D-printed biocarriers; Kaldnes K1 biocarriers; 13X-halloysite biocarriers; membrane fouling; SMP; EPS; colloidal particles; wastewater treatment

1. Introduction

Using Moving Bed Biofilm Reactors (MBBR) is the most simple and commonly used method for applying biocarriers during aerobic wastewater treatment [1]. However, certain limitations of MBBRs have led to the use of a hybrid model in which MBBRs are combined with other advanced wastewater treatment technologies, such as membrane bioreactors (MBR). The combination of MBBR-MBR was found to be more effective than MBR in terms of pollutant removal [2]. The advent of MBBR and MBR in the latter part of the 20th century has revolutionized research in the field of wastewater treatment [2–4]. The use of MBBR-MBR processes has shown promising results for the circular economy due to their high nutrient removal and recovery potential [3]. MBBR-MBR processes are financially and environmentally competitive methods, as they do not require the constant addition of costly reagents and they do not produce dangerous residuals [1,5,6]. This is, therefore, an advanced low-cost technology while at the same time it is also simple, reliable as well as stable to use, and it allows all processes to take place in one tank [7]. Despite the multiple advantages of MBBR-MBR use, there is one important disadvantage. In MBR technology, membrane fouling occurs, which is the unwanted deposit of suspended particles, colloidal and soluble components of mixed liquor on the surface and on the inside of the filtration membrane pores [8–10]. This phenomenon causes the transmembrane pressure to increase something that reduces the MBR performance resulting in the increase of operating and maintenance costs.

Some of the main components of the activated sludge, which are also the most important membrane foulants, are the Soluble Microbial Products (SMP) and the Extracellular Polymeric

 doi:10.20944/preprints202306.0393.v1

Substances (EPS) [11]. The production of SMP and EPS is a typical process for microorganisms in their natural environment. SMP and EPS comprise a gel-like biofilm matrix that is particularly hydrated and often electrically charged, in which microorganisms are integrated and immobilized [12]. The mixed liquor of activated sludge also contains colloidal components which according to recent studies are also an important membrane foulant [13].

Nowadays, freely moving submerged biocarriers in aeration tanks are used in modern MBBR methods, combining two different processes: the processes of attached and suspended biomass growth. With this technology, the processes of biodegradation of organic pollutants, nitrification, denitrification and ammonia removal are carried out [14,15]. In MBBR, each biocarrier increases the wastewater treatment performance by providing a protected surface for the growth of autotrophic and heterotrophic microorganisms and thus achieving high rates of degradation. For the MBBR to function properly, a steady-state biofilm should be formed on the surface of the biocarriers [16].

Various methods have been studied and used to deal with the issue of filtration membranes fouling, one of which is the addition of biocarriers. Biocarriers are added with the aim of performing an immediate abrasion of the membrane surface as they move in the membrane tank due to aeration, as long as they are put in the membrane tank, and on the other hand they are added with the aim of reducing the sludge metabolism products, meaning the SMP and EPS, due to their attachment to the biofilm. Lee et al. (2021) [17] used granule activated carbon biocarriers combined with Kaldnes K3 biocarriers modified by inserting a sponge cube and found out that the additional internal recirculation improved the effluent quality further, by increasing the nitrogen removal. Membrane filterability improved as well, by reducing the cake layer resistance. Sun et al. (2021) [18] used K1 commercial biocarriers and produced an effluent of excellent quality. Moreover, the fouling of the ceramic membrane was reduced, a result attributed among others to the fluidized biocarriers, reducing energy consumption by 44%.

Biofilm thickness is one the main parameters used when evaluating the MBBR performance. Studies have suggested that in a more than 700 μm thick biofilm nitrogen removal cannot be sustained due to the lack of substrate in the deep anaerobic layer. A critical parameter that determines the efficiency of MBBR technology is the appropriate design of the biocarrier [19]. The optimal biocarriers should have a large specific surface per volume unit. Other biocarrier characteristics that significantly affect the MBBR performance are the material they are made of, their surface characteristics, their orientation, the distance among the pores and their geometry [20,21]. The large specific surface and the strong interactions of the bacterial surface are the two main criteria for the creation of high-performing biocarriers. Large specific surface area may increase volumetric loads of biomass, while strong bacterial surface interactions may prevent biofilm detachment caused by external hydraulic forces [22].

3D printing technology is the solution to the problem of designing the optimal biocarrier by offering flexibility in its design and in the selection of its manufacturing material. A first attempt to construct 3D-printed biocarriers and use them in an MBBR unit was made by Elliott et al. (2017) [21] and by Tang et al. (2017) [23] in which the efficiency of this technology for the improvement of biocarrier characteristics in MBBRs was proven. Dong et al. (2015) [15], fabricated a series of 3D biocarriers in the shape of hollow honeycomb spherical structures for COD and NH_3 removal. Elliot et al. (2017) [21] succeeded in increasing the NH_3 removal rate by 1,620 ppm/d as compared to common biocarriers by creating spherical biocarriers with a larger specific surface area. There are also promising results in current studies regarding the unique advantages of 3D-printing for the fabrication of biocarriers with the purpose of the production of biofilm highly-loaded with dry mass and/or bio-activities. Chioti et al (2022) [24], have found a remarkable wastewater treatment efficiency when studying the performance of Kaldnes K1 biocarriers and various 3D-printed 13X biocarriers in aerobic wastewater treatment lab reactors of an active volume of 150 mL.

Aim of the study was the comparative evaluation of the MBBR-MBR unit's performance during urban wastewater treatment under the following three conditions: the addition of 3D-printed biocarriers fabricated from 13X and halloysite, the addition of Kaldnes K1 commercial biocarriers and

 doi:10.20944/preprints202306.0393.v1

the non-addition of biocarriers. In addition, the effect of biocarriers on the membrane fouling mechanism was also studied.

2. Materials and Methods

2.1. MBBR-MBR Set-up and Operating Conditions

For the purposes of this research, a semi-pilot MBBR was used combined with an MBR, with a total active volume of 15 L, the flow diagram of which is shown in **Figure 1**. The unit consisted of a synthetic wastewater storing tank, two aerated tanks of the same volume one after the other and a membrane tank. In the membrane tank there was also a submerged hydrophilic flat sheet A4 microfiltration membrane (Kubota). At the bottom of the membrane tank, intense aeration was applied, so that the cake layer that was formed on the membrane surface is removed. The filtration flow was intermittent with 10 minutes of operation and 2 minutes of pause. The synthetic sewage was prepared twice a week and had the following composition: glucose (500 mg/L), corn starch (500 mg/L), NH_4Cl (200 mg/L), peptone (56 mg/L), KH_2PO_4 (53 mg/L), $MgSO_4 \cdot 7H_2O$ (18 mg/L), $MnSO_4 \cdot H_2O$ (7.4 mg/L), $FeSO_4 \cdot 7H_2O$ (1.1 mg/L) and $NaHCO_3$ (240 mg/L) [9,13]. At the start of the experiment, activated sludge from a wastewater treatment plant in Thessaloniki was added to the MBBR-MBR tank for the acclimatization of the synthetic sewage.

The MBBRs consisted of 2 dissolved oxygen measuring devices, 3 peristaltic pumps, an air compressor, a thermometer and a PLC system (Eutech Instruments), which was used for documenting and setting the operation parameters with the help of SCADA software (Simantec, Siemens). The parameters documented and set via the SCADA software were: influent (Q_{IN}=0,9 L/h), recirculation (Q_r=2,1 L/h), effluent (Q_{OUT}=1,1 L/h), temperature, dissolved oxygen concentration in the two aerated tanks, and transmembrane pressure drop.

Three continuous flow experiments were conducted each one lasting more than one month. No biocarriers were added to the unit in the first experiment and therefore it will be hereinafter referred to as **control MBBR-MBR**. During the second experiment, commercial Kaldnes K1 biocarriers were added in the first aerated tank of the MBBR-MBR unit (**Figure 2a**) with a total volume of 1 L. This experiment will be hereinafter referred to as **MBBR-MBR K1**. 3D-printed biocarriers manufactured with 13X with halloysite (**Figure 2b**) were added in the second experiment also in the first aerated tank of the MBBR-MBR unit with a total volume of 1 L. This experiment will be hereinafter referred to as **MBBR-MBR 13X-H**. The percentage of biocarriers added is 20% of the first aerated tank of the MBBR-MBR unit or to 7% of the whole MBBR-MBR unit.

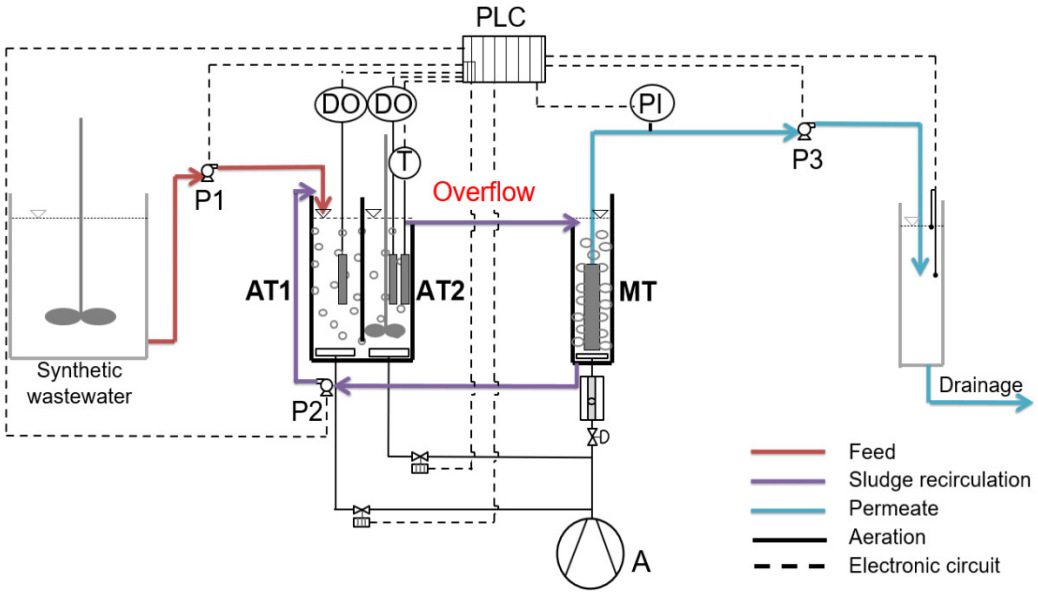

 doi:10.20944/preprints202306.0393.v1

Figure 1. MBBR-MBR flow diagram in which: AT1: 1st aerated tank (V_{AT1}=5 L), AT2: 2nd aerated tank (V_{AT2}=5 L), MT: membrane tank (V_{MT}=5 L), A: air Compressor, DO: dissolved oxygen measuring device and PLC: programmable logic controller, T: temperature measurement, PI: pressure indicator, P1, P2, P3: peristaltic pumps.

In all three MBBR-MBR units, synthetic wastewater with a similar COD inflow amount (779±85 mg/L for control MBBR-MBR, 772±98 mg/L for MBBR-MBR K1 and 780±84 mg/L for MBBR-MBR 13X-H) was used. It was also made sure that the activated sludge mixed liquor contained a similar amount of MLSS in all three units (5.9±0.4 g/L for control MBBR-MBR, 6.2±0.7 g/L for MBBR-MBR K1 and 5.8±0.7 g/L for MBBR-MBR 13X-H). To maintain the MLSS values, regular measurements took place and, depending on the results, mud was either added or removed. The dissolved oxygen in the two aerated tanks was kept to 2.5 mg/L in all three MBBR-MBRs, so that the aerobic biodegradation of the wastewater is efficient. Finally, in all three experiments, there were also similar F/M ratio values (0.19 g COD/g MLSS/d for control MBBR-MBR, 0.18 g COD/g MLSS/d for MBBR-MBR K1 and 0.19 g COD/g MLSS/d for MBBR-MBR 13X-H). The above were decided with the purpose of enabling the comparison of the three experiments.

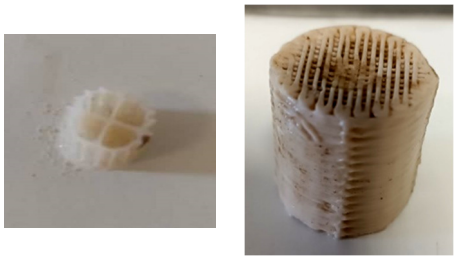

(**a**) (**b**)

Figure 2. (**a**) Commercial Kaldnes K1 biocarriers and (**b**) 3D-printed biocarriers fabricated with 13X and halloysite.

2.2. Biofilm Extraction Method

Draw of biocarrier samples from the MBBR-MBR and biofilm extraction from their surfaces were regularly performed with the purpose of determining the dry mass, the MLSS, the SMPs and the EPS. The extraction of biofilm was carried out using the Mandakhalikar et al. (2018) [1,7] method, which includes placing the biocarrier sample in 10 mL of deionized water, stirring it in a vortex device for 1 minute, placing it in an ultrasonic device for 2 minutes and then repeating the stirring in a vortex device for another minute. This methodology contributed to the complete removal of the biofilm.

2.3. Printing Methodology of the 3D-Printed Biocarriers with 13X with Halloysite

The preparation of the printing paste included the mixing of the ceramic material (13X), the inorganic (halloysite) and the organic binders in a mortar to the point where the mixture of solid content was homogenized. Afterwards, deionized water was mixed with the colloidal silica. Finally, the mixture of liquid content was gradually added to the mixture of solids, while at the same time it was being fused with a pestle until the paste to achieve homogenization. To remove all aggregates and grains from the paste, the mixture was sieved in a 45μm-hole-diameter sieve. **Table 1** below shows the zeolite and inorganic binders proportions.

Table 1. Proportions of zeolite paste and clay binding medium.

	Material	**Paste content**	**Zeolite/clay percentage**
Zeolite	13X	50%	89%
Inorganic binder	Halloysite nanotubes	6%	11%
Colloidal silica	Ludox AS-40	16%	
	Water	27%	

 doi:10.20944/preprints202306.0393.v1

Organic binder	Methyl cellulose	1%

Centrifugation took place to ensure the removal of any air bubbles, transferred to the syringe and finally to the printer. Then, the process of preparing the printer took place. This process included the creation of the biocarriers 3D geometry, during which parameters like the shape, the recurring geometric pattern, the height of each layer, the nozzle diameter, the pressure and the printing speed were determined. Cylinder was chosen as the recurring geometric pattern for the biocarriers and the dimensions of the biocarrier were: 13 mm width, 13 mm length, 20 mm height and 4.8564 g weight. An in-house CNC printer was used for the printing.

2.4. Determination of the Physicochemical Parameters

The physicochemical parameters used in the influent and effluent wastewater characterization (COD, Total N, NH_4-N and NO_3-N) were determined using Hack–Lange LCK kits, along with a DR-2800 spectrophotometer. Mixed liquor suspended solids (MLSS) were measured according to standard methods [25]. The measurements were performed regularly to evaluate the progress of the experiments and the efficiency of MBBR-MBR treatment.

Regular measurements, documentation and setting of dissolved oxygen also took place, using a Greisinger OXY 3610 MP measuring electrode.

Samples were taken from the membrane tank and the effluent on a regular basis to measure the SMPs and EPS. For SMP and EPS extraction, a natural thermal extraction method was used [8,26]. Then, the extracted SMPs and EPS in the form of proteins were measured using the modified Lowry method and repeating it three times [27], while the SMPs and EPS in the form of carbohydrates were measured using the photometric method proposed by Dubois et al. (1956) [28] and repeating it two times. The protein calibration curve was prepared using Bovine Serum Albumin (BSA, Sigma Aldrich) and the carbohydrates calibration curve was prepared using glucose (Panreac).

Dynamic light scattering (Brookhaven Instruments) was used to determine the size distribution of the less than 1 μm coloidal particles of the membrane tank and the effluent. Static light scattering (Mastersizer, Malvern) was used to determine the size distribution of aggregates with a diameter larger than 10 μm. Activated sludge and effluent were also observed under a Light Sheet Microscope (LSM, Observer Z1, Zeiss, Oberkochen, Germany) and filamentous index (FI) evaluation was also performed [29,30], in order to measure the population of filamentous microorganisms in the activated sludge mixed liquor. The microscope images were edited using ZEN software.

2.5. DNA Extraction and 16S rRNA Gene Amplicon Sequencing

DNeasy PowerSoil Pro Kit (QIAGEN, Hilde, Germany) was employed to extract genomic DNA from the biofilm suspensions according to the manufacturer's guidelines. Library preparation for sequencing of the 16S rRNA gene was carried out based on the standard 16S Metagenomic Sequencing Library Preparation protocol (IlluminaTM, Inc., San Diego, CA, United States). Specifically, the V3-V4 hypervariable regions of the 16S rRNA gene were targeted using the 341f/805r primer pair (341f 5′-CCTACGGGNGGCWGCAG-3′, 805r 5′-GACTACHVGGTATCTAATCC-3′). The resulting DNA libraries were quantified with a Qubit™ 4 Fluorometer (Thermo Fisher Scientific, Waltham, MA, USA), and their size was confirmed by electrophoresis on a 1.5% agarose gel. The libraries were equimolarly pooled, and their concentration was assessed by quantitative PCR using the QIAseq Library Quant Assay Kit (QIAGEN, Germany). The pooled library was spiked with 25% phiX control library (Illumina Inc., San Diego, CA, USA), denatured, and diluted to a final concentration of 6 pM. Sequencing was carried out on an Illumina MiSeqTM platform with either the MiSeq Reagent Nano Kit version 2 (500-Cycle) or the MiSeq Reagent Kit version 3 (600-Cycle) chemistry for a paired-end, 2x250-bp or 2x300 cycle run.

 doi:10.20944/preprints202306.0393.v1

2.6. Bioinformatics

To analyze the data obtained from the sequencing, the Quantitative Insights Into Microbial Ecology 2 (QIIME2) software, version 2022.2 [31] was used. The DADA2 algorithm [32] was utilized for quality-based trimming, filtering, and chimera detection and removal, resulting in the construction of Amplicon Sequence Variants (ASV). Taxonomic annotation of the reads was performed using the SILVA reference database (SSU, release 138) [33]. For alpha and beta diversity analysis, the q2-diversity plugin was utilized to calculate several metrics and generate principal coordinates analysis (PCoA) plots using Emperor for each beta diversity. Faith's Phylogenetic Diversity and weighted and unweighted UniFrac were used to measure phylogenetic diversity.

3. Results

3.1. Evaluation of the MBBR-MBR Performance for the 3 Units

Figure 3 shows the transmembrane pressure (TMP) diagrams in relation to time for all three MBBR-MBR units and **Figure 4** shows the COD results for the influent and effluent waste.

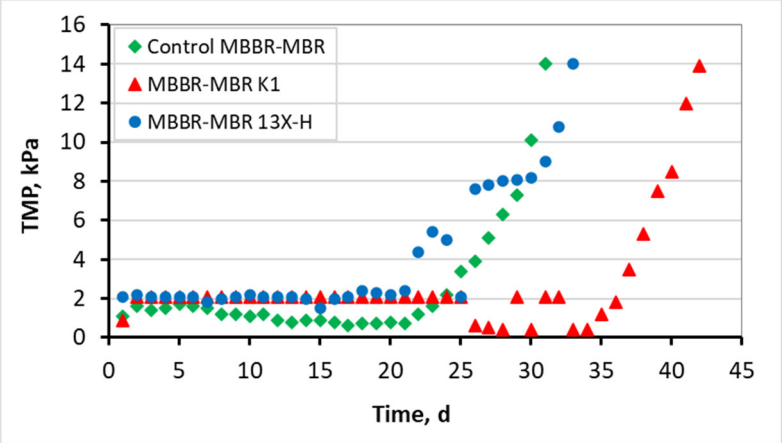

Figure 3. Transmembrane pressure (TMP) in relation to operating time for the control MBBR-MBR, the MBBR-MBR K1 and the MBBR-MBR 13X-H.

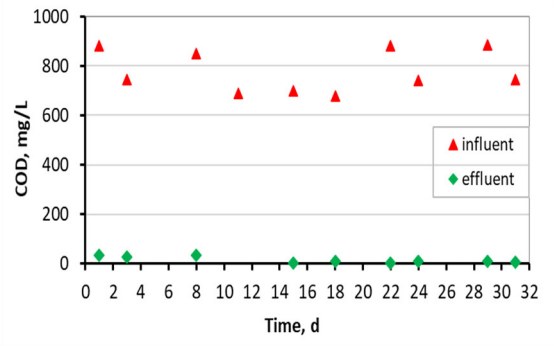

(**a**)

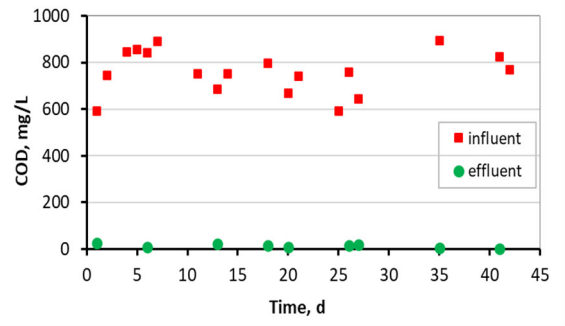

(**b**)

Preprints.org (www.preprints.org) | NOT PEER-REVIEWED | Posted: 6 June 2023 doi:10.20944/preprints202306.0393.v1

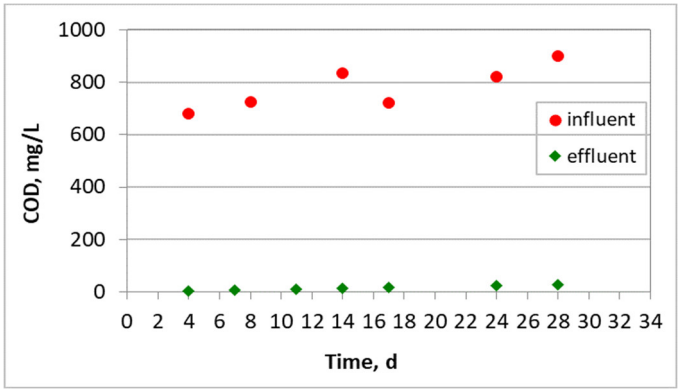

(c)

Figure 4. COD in relation to operating time for (**a**) the control MBBR-MBR, (**b**) the MBBR-MBR K1 and (**c**) the MBBR-MBR 13X-H.

Figures 5–7 present the NO_3-N, NH_4-N and Total N results for the influent and effluent waste in all three MBBR-MBR.

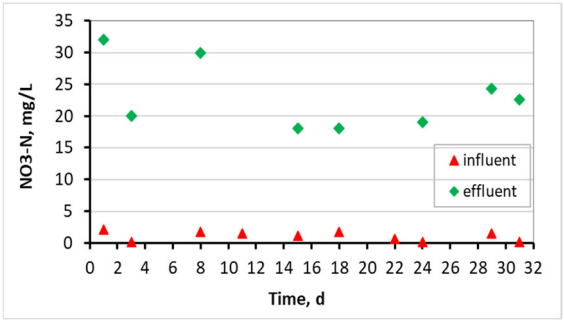

(a)

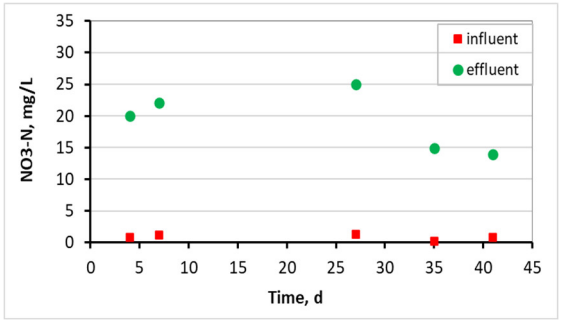

(b)

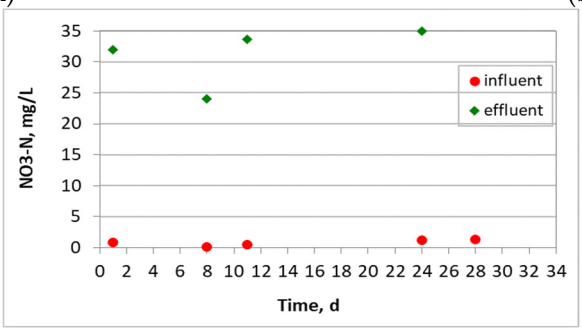

(c)

Figure 5. NO_3-N in relation to operating time for (**a**) the control MBBR-MBR, (**b**) the MBBR-MBR K1 and (**c**) the MBBR-MBR 13X-H.

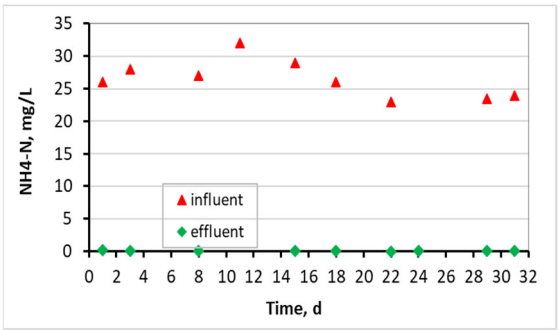

(a)

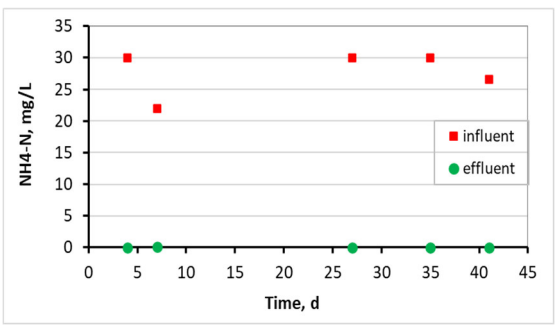

(b)

Preprints.org (www.preprints.org) | NOT PEER-REVIEWED | Posted: 6 June 2023 doi:10.20944/preprints202306.0393.v1

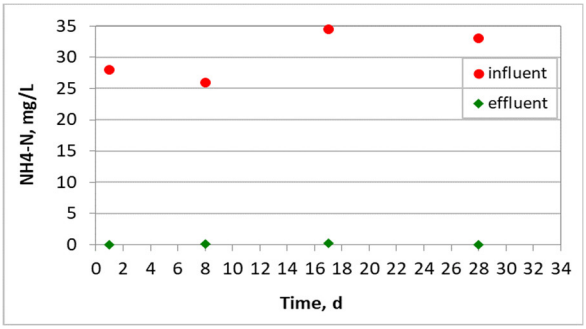

(c)

Figure 6. NH_4-N in relation to operating time for (**a**) the control MBBR-MBR, (**b**) the MBBR-MBR K1 and (**c**) the MBBR-MBR 13X-H.

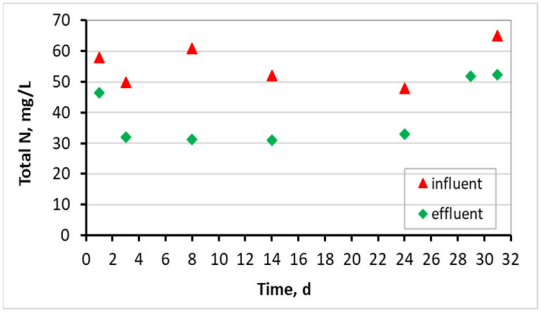

(a)

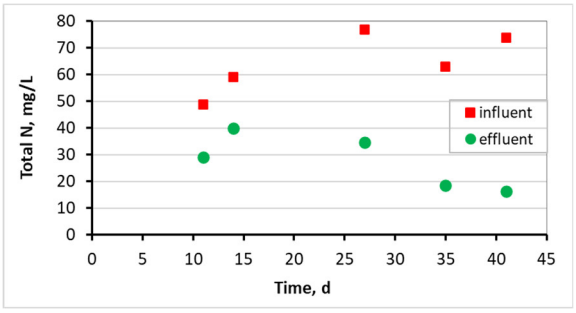

(b)

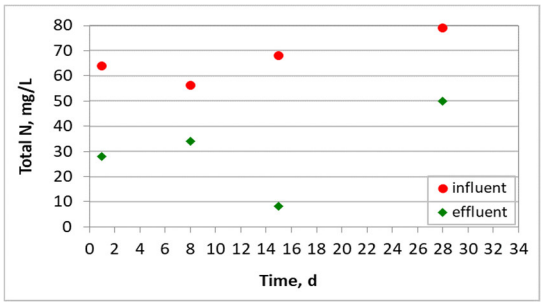

(c)

Figure 7. Total N in relation to operating time for (a) the control MBBR-MBR, (b) the MBBR-MBR K1 and (c) the MBBR-MBR 13X-H.

Figures 8 and 9 show the SMP proteins and SMP carbohydrates concentration diagrams for mixed liquor in the membrane tank and the effluent in all three MBBR-MBR.

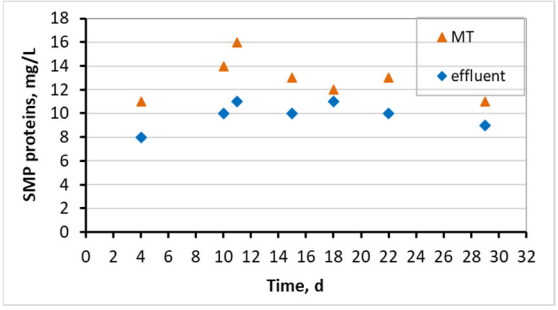

(a)

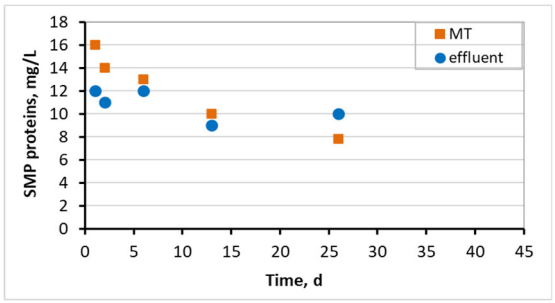

(b)

Preprints.org (www.preprints.org) | NOT PEER-REVIEWED | Posted: 6 June 2023 doi:10.20944/preprints202306.0393.v1

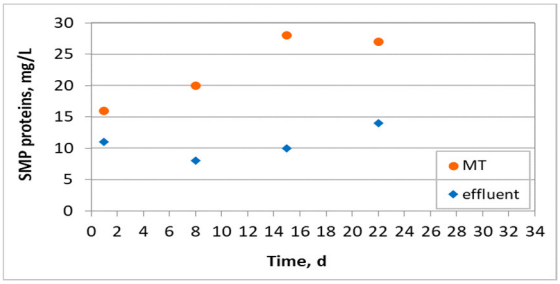

(c)

Figure 8. Concentration of SMP proteins in the membrane tank (MT) and effluent in relation to operating time for the (a) control MBBR-MBR, (b) MBBR-MBR K1 and (c) MBBR-MBR 13X-H.

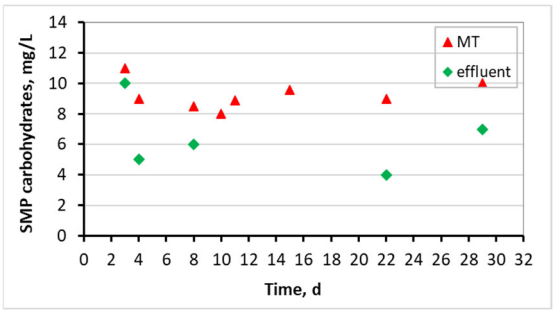

(a)

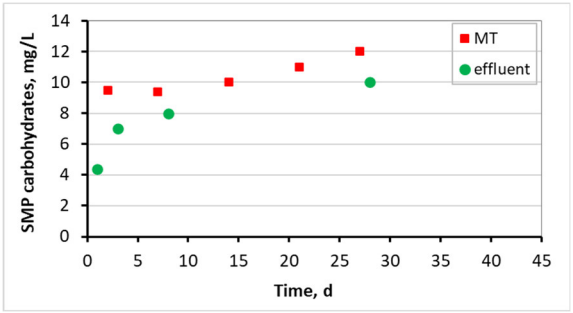

(b)

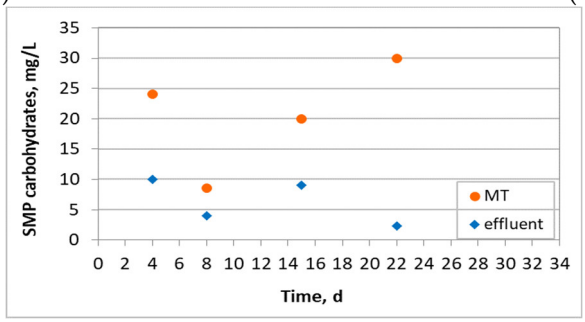

(c)

Figure 9. Concentration of SMP carbohydrates in the membrane tank (MT) and effluent in relation to the operating time for the (**a**) control MBBR-MBR, (**b**) MBBR-MBR K1 and (**c**) MBBR-MBR 13X-H.

Figure 10a shows a standard optical microscope image of the activated sludge mixed liquor and **Figure 10b** shows a standard optical microscope image of the effluent in MBBR-MBR units. The average aggregates size in the mixed liquor ranged to 325 μm in control MBBR-MBR, to 139 μm in MBBR-MBR K1 and to 306 μm in the mix MBBR-MBR 13X-H in the mixed liquor of the first aerated tank.

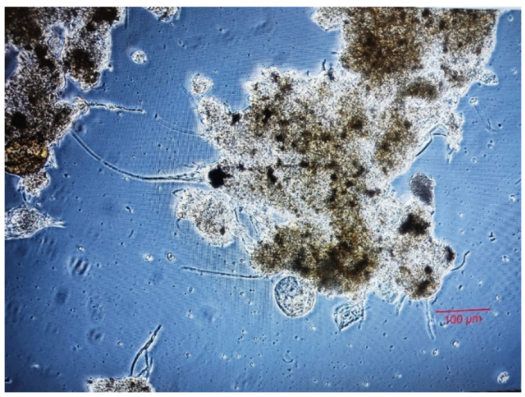

(a)

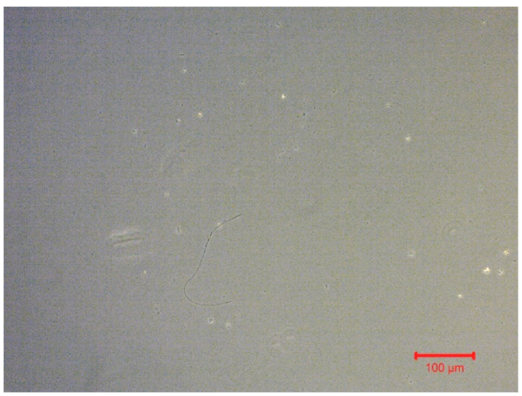

(b)

Figure 10. Standard images of optical microscope for (**a**) the mixed liquor and (**b**) the effluent.

 doi:10.20944/preprints202306.0393.v1

Figure 11 shows the ≤400 nm-sized-colloidal particles rates for the mixed liquor in the membrane tank and for the effluent in all 3 MBBR-MBR units.

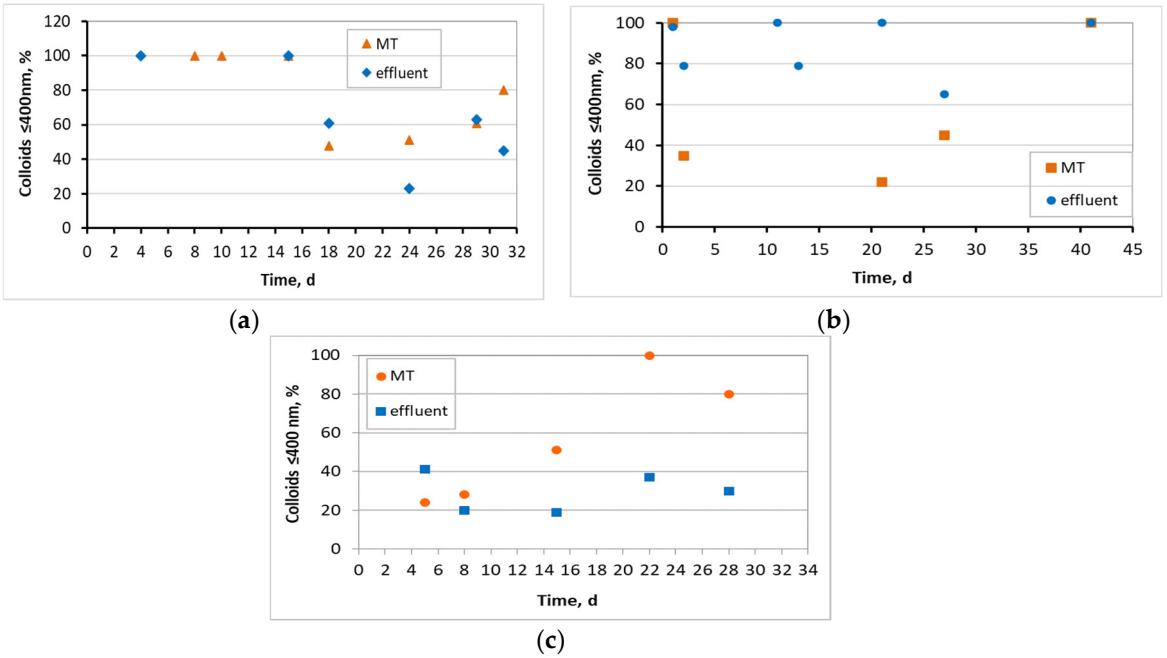

Figure 11. Percentage of colloidal particles with size ≤400 nm in relation to the operating time for the membrane tank (MT) and effluent in (**a**) the control MBBR-MBR, (**b**) the MBBR-MBR K1 and (**c**) the MBBR-MBR 13X-H.

3.2. Biofilm Evaluation for the Kaldnes K1 Biocarriers

Figure 12 shows the biocarriers and the biofilm that was developed on the inside of the biocarriers' surfaces in relation to the operating time of the MBBR-MBR K1 unit. **Table 2** shows the dry mass and MLSS concentration measurements in the biofilm that was developed on the surfaces of the biocarriers. The measurements were the result of the average biofilm value that was developed in three biocarriers per day of measurement.

Figure 12. Biocarriers with the formed biofilm on the (**a**) 6th day, (**b**) 27th day and (**c**) on the 48th day of the MBBR-MBR K1 operation. .

Table 2. Dry mass and MLSS concentration values of the biofilm developed in the biocarriers in relation to the operating time of the unit.

t, d	Dry Mass of Biofilm, mg	MLSS, mg/L
6	3.2	40
20	3.5	240
32	4.6	360
41	2.9	20

Figure 13 presents the SMP and EPS protein and carbohydrates concentration for the biofilm of the biocarriers in relation to the time after biofilm extraction from four biocarriers per day.

 doi:10.20944/preprints202306.0393.v1

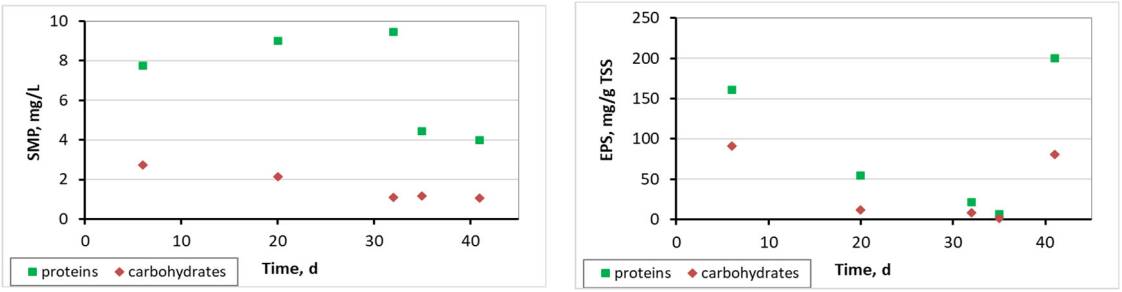

(**a**) (**b**)

Figure 13. (**a**) SMP and (**b**) EPS protein and carbohydrates concentration in the biofilm of the biocarriers in relation to time.

3.3. Biofilm Evaluation for the 3D-Printed 13X and Halloysite Biocarriers

Figure 14 shows the biocarriers and the biofilm that was developed on the inside of the biocarriers' surfaces in relation to time. **Table 3** shows the dry mass and MLSS concentration measurements in the biofilm that was developed on the surfaces of the biocarriers. The measurements were the result of the average biofilm value that was developed in three biocarriers per day of measurement.

(**a**) (**b**) (**c**)

Figure 14. Biocarriers with the formed biofilm on the (**a**) 11th day, (**b**) 15th day and (**c**) 24th day of the MBBR-MBR 13X-H operation.

Table 3. Dry mass and MLSS concentration values of the biofilm developed in the biocarriers in relation to the operating time of the unit.

t, d	Dry mass, mg	MLSS, mg/L
11	4,980	863
14	5,426	1,875
24	5,210	1,038
28	5,711	1,250

Figure 15 shows the SMP and EPS protein and carbohydrates diagrams for the biofilm of the biocarriers in relation to the time, after biofilm extraction from four biocarriers per day of measurement. Finally, **Figure 6** presents the fragments of 13X-H biocarriers at the end of the experiment.

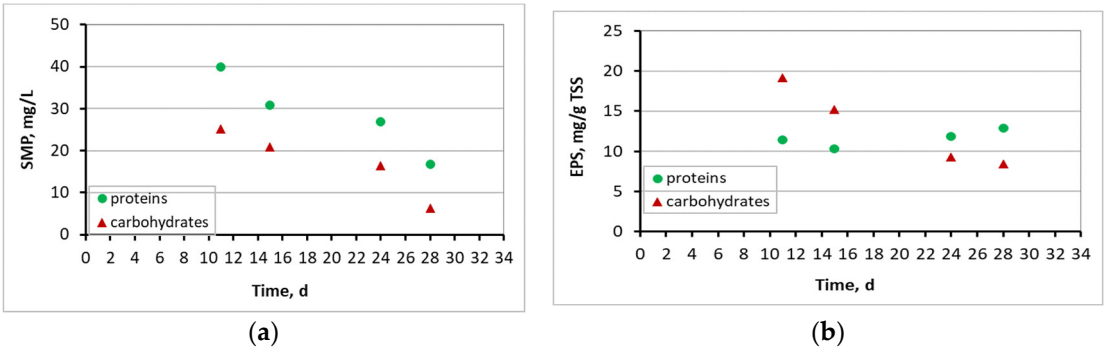

(**a**) (**b**)

 doi:10.20944/preprints202306.0393.v1

Figure 15. (**a**) SMP and (**b**) EPS protein and carbohydrates concentration in the biofilm of the biocarriers in relation to time.

Figure 16. 13X-H biocarriers fragments at the end of the experiment.

3.4. Microbiome Analysis on Biofilm of Biocarriers via 16S rRNA Sequencing

The findings from the microbiome analysis of the biofilm developed on K1 and 3D-printed biocarriers using 16S rRNA sequencing on day 30 of operation indicated that *Proteobacteria* (34.2-37.2%), *Actinobacteria* (9.6%-19.3%), *Bacteroidetes* (8.4%-16.9%), *Firmicutes* (2.8%-9.9%), *Chloroflexi* (3.2%-6.7%), and *Planctomycetes* (6%-6.5%) were among the most abundant phyla. *Alphaproteobacteria* (19.4%), together with *Actinobacteria* (19.3%) dominated in the 3D-printed biocarriers, followed by *Gammaproteobacteria* (9.7%), *Planctomycetia* (6.5%), *Bacilli* (5.3%), and *Betaproteobacteria* (4.5%). *Alphaproteobacteria* (11.2%) were also dominant in K1 ring, along with *Betaproteobacteria* (10.9%), *Actinobacteria* (9.6%), *Sphingobacteriia* (9%), *Gammaproteobacteria* (8.2%), and *Planctomycetia* (5.8%). As regards the families, the biofilm on 3D-printed biocarriers was mainly composed of *Planctomycetaceae* (6.5%), *Xanthomonadaceae* (4.4%), *Rhodobacteraceae* (4.3%), and *Mycobacteriaceae* (3.7%). Similarly, *Planctomycetaceae* (5.8%) and *Xanthomonadaceae* (5.1%) were also enriched in K1 carrier, however the overall profile was different, with *Deinococcaceae* (5.3%), *Saprospiraceae* (4.9%), *Rhodocyclaceae* (4.8%), *Caldilineaceae* (4.5%), and *Comamonadaceae* (4.2%) being the most abundant. At genus level, 3D-printed biocarriers were mainly characterized by *Mycobacterium* (3.5%), followed by *Trichococcus* (2.3%), *Solirubrobacter* (2.2%), *Litorilinea* (2%), *Rudanella* (1.8%), and *Saccharibacteria* genera incertae sedis (1.8%). Conversely, in the biofilm of K1 ring the major genera were *Deinococcus* (5.3%), *Runella* (3%), *Litorilinea* (2.9%), *Nitrospira* (2.4%), *Armatimonadetes* gp5 (2.3%), *Lewinella* (2%), and *Micropruina* (1.9%). **Figures 17** and **18** show the most prevailing families and genera, respectively, detected within the biofilm of K1 and 3D-printed biocarriers.

 doi:10.20944/preprints202306.0393.v1

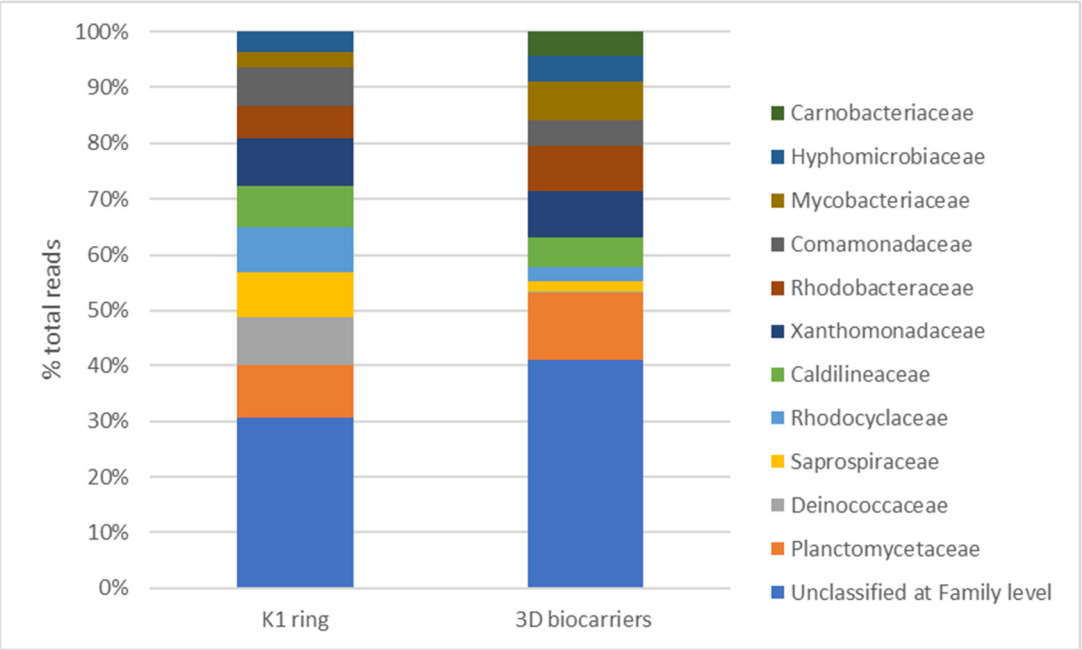

Figure 17. Relative abundance of the core families found on the biofilm of K1 ring and 3D-printed biocarriers at 30 days of operation.

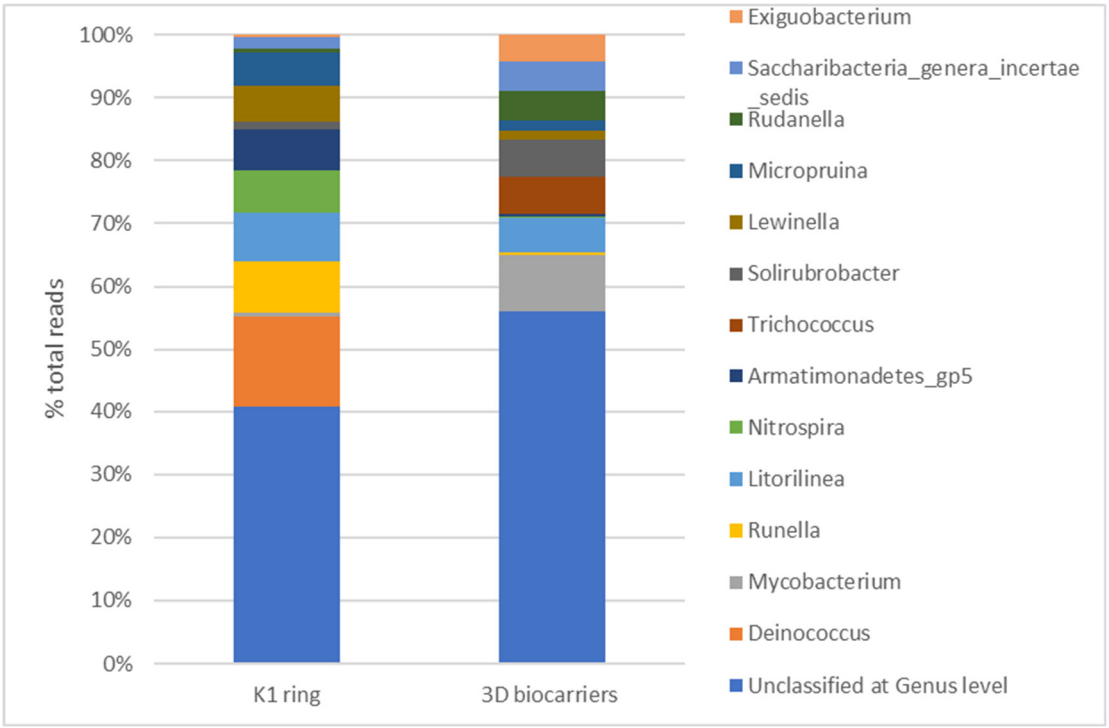

Figure 18. Relative abundance of the core genera found on the biofilm of K1 ring and 3D-printed biocarriers at 30 days of operation.

4. Discussion

The MBBR-MBR units were operating under an F/M loading of 0.18-0.19 g COD/g MLSS/d, which is within the desirable value range for an efficient wastewater treatment. As shown in **Figure 3**, the transmembrane pressure (TMP) was maintained lower than 2 kPa until the 24th day of unit operation and full total membrane fouling was reached on the 31st day of unit operation. With the addition of commercial Kaldnes K1 biocarriers, a remarkable improvement of filtration was observed, and the membrane fouling took place 11 days later. More specifically, the TMP was

 doi:10.20944/preprints202306.0393.v1

maintained lower than 2 kPa until the 36th day of unit operation and the total membrane fouling took place on the 42nd day of unit operation. With the addition of 13X-H 3D-printed biocarriers, TMP increased more than 2kPa on the 21st day, while the total fouling took place on the 33rd day of unit operation. Therefore, the addition of 13X-H biocarriers allowed a membrane filtration of the same degree as in control MBBR-MBR, not showing any substantial improvement or deterioration. Despite the fact that the addition of 13X-H biocarriers contributed to the successful growth and protection of a significant amount of biofilm on their surfaces, it was not enough to improve the performance of membrane filtration. This is attributed to the fact that a small part of the biocarriers got fragmented due to the aeration of the tank, which led to the scattering of tiny particles of halloysite in the mixed liquor, particles which, judging by the results, were most probably driven to the membrane pores and blocked them. Another reason for this result of the addition of 13X-H biocarriers is the production of a large amount of SMP (**Figures 8** and **9**) resulting from a great creation of biofilm on the biocarriers (**Table 3**). Other researchers have also observed this result for other types of biocarriers in MBBR-MBR units [2,34].

Based on **Figure 4** and on the influent and effluent COD values, it can be concluded that there is an excellent effluent quality in all three MBBR-MBR units, with a COD removal rate of 98% for all units. NO_3-N in the effluent of the unit was increased in control MBBR-MBR as much as it was increased in MBBR-MBR K1 (95%). The increase of NO_3-N was slightly better in MBBR-MBR 13X-H as it was 97.5% (**Figure 5**). NH_4-N concentration was significantly reduced reaching 0 mg/L meaning that the removal rate reached approximately 100% in all three MBBR-MBRs (**Figure 6**). Finally, 29% of Total N was removed from control MBBR-MBR while 57% of Total N was removed from MBBR-MBR K1 showing a clear improvement (**Figure 7**). 55% of Total N was removed from MBBR-MBR 13X-H meaning that the removal in MBBR-MBR 13X-H was better than in the control MBBR-MBR and slightly less than MBBR-MBR K1. It can, thus, be concluded that the processes of nitrification and denitrification were enhanced with the addition of K1 and 13X-H biocarriers in the MBBR-MBR unit in relation to control MBBR-MBR, as the MBBR incorporates the advantages of both suspended and attached growth process where microorganisms grow on biocarriers in the form of biofilm [35]. The biofilm formed on biocarriers includes the existence of anoxic/anaerobic inner layers and aerobic outer layers. Therefore, nutrient removal is accomplished in a single reactor reducing the land area requirement for wastewater treatment plant. An excellent effluent quality in relation to COD, NH_4-N and Total N removal, was mentioned in other studies as well [3,36]. Wastewater treatment performance similar to the one in the current experiment was observed with the only difference being the use of bigger filling ratios (0.35-0.67) as opposed to this experiment in which 0.20 filling ratio was used.

Figures 8 and **9** indicate the SMP protein and carbohydrates concentration in all three reactors. In control MBBR-MBR and in MBBR-MBR K1 it was found that many SMP exits into the filtrate, something that was not observed in MBBR-MBR 13X-H, as a smaller amount of SMP exits into the filtrate. Most likely, this is due to the fact that, as discussed below, more biofilm is developed in 13X-H biocarriers than in K1 biocarriers. As a result, SMP are kept on the inside of the biofilm and prevents the SMP to exit into the filtrate (**Figure 15**). This finding plays a significant role in the improvement of the filtrate membrane performance because the SMP are one of the most important membrane foulants. More specifically, in control MBBR-MBR the SMP protein concentration was 13 mg/L and the SMP carbohydrates concentration was 9.3 mg/L. In MBBR-MBR K1 the average values of SMP were similar to the values in control MBBR-MBR, with the protein concentration being 13 mg/L and the SMP carbohydrates concentration 10 mg/L. In MBBR-MBR 13X-H, the average values of SMP increased by approximately 10 units as compared to the other experiments, with the SMP protein concentration being 23 mg/L and the SMP carbohydrates concentration being 21 mg/L. As mentioned before, this is due to the increased biofilm production in the 13X-H biocarriers. This phenomenon is, on the one hand, beneficial, as it improves the performance of wastewater treatment but on the other, it leads to an increase of the generated SPM which are basic foulants for the filtration membrane. Similar results for other types of biocarriers in MBBR-MBR units were also found by other researchers [2,34], who tried to fix this issue by applying intermittent voltage in the membrane tank.

 doi:10.20944/preprints202306.0393.v1

Filamentous microorganisms protruding from the sludge flocs are observed in the mixed liquor photograph drawn by an optical microscope (**Figure 10a**). This shows that the filamentous index (FI) for the specific sludge ranges from 1-2 during the entire operation of all three MBBR-MBR units [29]. On the optical microscope image in **Figure 10b** it is shown that quite large aggregates and filamentous microorganisms exit into the filtrate.

The size of aggregates in activated sludge at the 1st aerated tank of the bioreactors was reduced from 325 μm in control MBBR-MBR to 139 μm in MBBR-MBR K1. This is attributed to the strong movement of K1 biocarriers due to aeration, which prevents the forming of large sludge flocculates and changes the sludge morphology. In MBBR-MBR 13X-H the size of the aggregates was reduced much less, and it reached 306 μm because the biocarriers agitation is much milder due to their increased weight.

In control MBBR-MBR, colloidal particles with ≤400 nm diameter, a diameter equal or less than the size of the membrane filtration pores, were observed to occupy 100% of the particles in the mixed liquor and the effluent until the 16th day of unit operation (**Figure 11a**). However, as the membrane fouling increases, the very small particles were reduced to a percentage less than 60-80%. In MBBR-MBR K1 fluctuations of the colloidal particles size were observed, something that can be explained by considering the respective fluctuations in the growing biofilm on the surfaces of the biocarriers (**Table 2**). The opposite trend was observed in MBBR-MBR 13X-H as compared to control MBBR-MBR. The colloidal particles concentration started low on 24% during the 5 days of unit operation and gradually increased reaching 80% on the 28th day of unit operation. The fragmentation of biocarriers and the leakage of tiny particles of halloysite inside the unit can explain the above result (**Figure 16**) and also the quick membrane fouling that took place (**Figure 3**).

Figure 12 shows that biofilm was clearly produced not only inside the K1 biocarriers, but also on the trabecular surfaces of the biocarriers' walls. Based on the values for the dry mass of the biofilm shown in **Table 2**, it can be concluded that it was gradually increased from 3.2 mg on the 6th day to 4.6 mg on the 32nd day. The dry mass of the biofilm was however reduced on the 41st day reaching 2.9 mg. A similar tendency is observed in the MLSS values. More specifically, their values changed increasingly from 40 mg/L on the 6th day of unit operation to 1100 mg/L on the 35th day. The MLSS value is reduced to 390 mg/L on the 41st day. In both cases, this fluctuation is attributed to the easy biofilm detachment from the large holes of K1 biocarriers. Due to the large opening the biocarriers cannot hold the biofilm stable and protected. The amount of SMP proteins that was created by the extraction of biofilm from the K1 biocarriers was gradually increasing over time (**Figure 13**). This increase matches the MLSS and biofilm increase on the surfaces of the biocarriers. Their decrease on the 35th to 40th days is linked to the biofilm detachment due to aeration. The same was also observed for the MLSS values. The SMP carbohydrates concentration was steadily low (less than 3 mg/L) and the EPS proteins and carbohydrates concentration was 160 mg/g. No correlation to the growing biofilm on the biocarriers was observed.

Biofilm was steadily grown on 3D-printed 13X biocarriers with halloysite, as shown in **Figure 14**. The large volume of biofilm is more easily observed in **Table 3** than by optical observation, as the biofilm tends to develop on the inside surface of the biocarriers which cannot be seen from the outside. According to **Table 3,** the dry mass of the biofilm values start from 4,980 mg on the 11th day of unit operation and steadily increase to 5,11 mg on the 28th day of unit operation. Compared to the K1 Kaldnes biocarriers, the increase of the developed biofilm was 3 orders of magnitude larger, something that is due to the 3D-printed biocarriers' design which included very small holes and large inside depth. It is also observed that the biofilm is safely maintained inside the biocarriers and does not detach as a result of the strong aeration in the aerated tank. This was not observed in K1 commercial biocarriers. The respective results also come from the MLSS units values, which were 863 mg/L on the 11th day of unit operation and were increased to 1,250 mg/L on the 28th day of unit operation. The fluctuations are due to the aeration of the units but they are negligible.

The SMP proteins on the biofilm of the 13X-H biocarriers increased by one order of magnitude and reached an average value of 29 mg/L as compared to the K1 biocarriers in which the average value was 7 mg/L (**Figure 15a**). The same increase was also noted for the SMP carbohydrates (1.5

 doi:10.20944/preprints202306.0393.v1

mg/L on the k1 biofilm and 17 mg/L on the 13X-H biofilm). On the contrary, the EPS proteins were significantly decreased from an average value of 12 mg/g TSS on the biofilm of 13X-H biocarriers to an average value of 62 mg/g TSS on the K1 biocarriers. Similarly, the EPS carbohydrates were reduced from an average value of 40 mg/g TSS on the K1 biocarriers to an average value of 13 mg/g TSS on the 13X-H. It is therefore concluded that EPS were mostly developed on the biofilm of the K1 biocarriers while more SMP were developed on the biofilm of 13X-H biocarriers than EPS.

Summing up, even though no mechanical agitation was used in the 1st aerated tank of the MBBR-MBR, a small fragment of a 13X-H biocarrier part was detected. This corresponds to 1/6 of the total biocarriers. Fragmentation was caused due to the strong aeration on the inside of the tank. The biocarriers fragments are shown on **Figure 16**.

The 16s rRNA sequencing analysis of the microbial communities growing on the tested biocarriers (**Figures 17** and **18**) revealed that *Alphaproteobacteria* was the most dominant for both kinds of carriers. Indeed, this class has been previously shown to effectively grow and prevail on various biocarrier types [37]. Members of this group, as well as from *Betaproteobacteria*, which had comparable abundance in K1 ring, but quite lower in 3D printed carriers, are linked to enhanced COD reduction and participate in denitrification and phosphate accumulation [38]. *Actinobacteria* were also highly present in both types of carriers, mediating propionate acid fermentation, as well as acetate and H_2 generation [39]. The most enriched genus found in K1 ring was *Deinococcus* (*Deinococcaceae*), almost absent in 3D biocarriers, which comprise a heterotrophic non-pathogenic aerobic group, able to survive extreme environmental conditions [40]. Though their role in aerobic digestion of activated sludge has not been yet documented, various species can degrade different carbohydrates and demand minimal media for their growth [40]. *Mycobacterium* (*Mycobacteriaceae*), on the other hand, prevailed in the case of 3D carriers as opposed to K1. Many *Mycobacterium* species have developed an adaptive mechanism to increase their ability to degrade contaminants in challenging environments. This is achieved by the presence of mycolic acids in their cell walls, which facilitate the effective adhesion and interaction with contaminants, especially when they are highly hydrophobic, thus enhancing their biodegradation process [41]. Therefore, the presence of these organisms in the biofilm of 3D carriers may indicate an improved organic contaminant removal from the system, contributing to overall process efficacy. Moreover, *Trichococcus*, which were copious in 3D-biocarriers, but barely detected in K1 ring, possess the ability to decompose benzene, an aromatic compound and common constituent of pesticides [42]. Consequently, it is possible that this bacterial group further promoted the biodegradation of pollutants in the system with 3D-biocarriers. It is worth noting, though, that *Nitrospira*, a major group of nitrite-oxidizing bacteria (NOB) [43], were more abundant in K1 ring than in 3D carriers. These bacteria have been previously reported to be the dominant NOB population in biofilms formed on K1 carriers used in combined systems of upflow blanket filter (UBF)-MBBR reactors [44].

5. Conclusions

In this study a comparative evaluation of the MBBR-MBR unit's performance during urban wastewater treatment was carried out under the following three conditions: when adding 13X-H biocarriers, when adding K1 biocarriers and when not adding biocarriers at all. In control MBBR-MBR the unit reached total membrane fouling on the 31st day of operation while in MBBR-MBR K1 unit there was a notable improvement of the filtration, and the membrane fouling was extended occurring on the 11th day. The addition of 13X-H biocarriers did not, however, cause any significant improvement of the filtration. This is attributed to the fact that 1/6 of the biocarriers got fragmented due to the aeration of the tank, which led to the scattering of tiny particles of halloysite in the mixed liquor, particles which blocked the membrane pores. More specifically, the colloidal particles concentration in MBBR-MBR 13X-H started low from 24% of the total number of particles and was gradually increased, reaching 80% on the 28th day of unit operation. Another reason that the membrane filtration was not improved with the addition of 13X-H biocarriers is the production of a large amount of SMP resulting from the large production of biofilm on the biocarriers. In control

 doi:10.20944/preprints202306.0393.v1

MBBR-MBR and in MBBR-MBR K1, the SMP concentration was 22 mg/L while in MBBR-MBR 13X-H the SMP were increased by approximately 10 units.

Based on the COD values, it can be concluded that there is an excellent effluent quality in all three MBBR-MBR units, with a COD removal rate of 98%. Finally, 29% of Total N was removed from control MBBR-MBR while 57% of Total N was removed from MBBR-MBR K1 and 55% from MBBR-MBR 13X-H, values that show a clear improvement. This means that the processes of nitrification and denitrification were enhanced with the addition of K1 and 13X-H biocarriers in the MBBR-MBR unit, as it incorporates the advantages of both suspended and attached growth. Finally, in the K1 biocarriers a small amount of biofilm was maintained which means that the biocarriers were easily detached from the large holes on K1 biocarriers. However, on 13X-H biocarriers, the biofilm production was increased by 3 orders of magnitude thanks to their correct design. It is finally concluded that mostly EPS were produced in the biofilm of K1 biocarriers and mostly SMP in the biofilm of 13X-H.

Author Contributions: Funding acquisition, Themistoklis Sfetsas; Investigation, Dimitra Banti; Methodology, Dimitra Banti, Eleni Kostopoulou and Vassiliki Tsioni; Software, Dimitra Banti; Supervision, Dimitra Banti, Petros Samaras and Themistoklis Sfetsas; Validation, Dimitra Banti, Petros Samaras, Eleni Kostopoulou and Vassiliki Tsioni; Writing – original draft, Dimitra Banti; Writing – review & editing, Dimitra Banti. All authors have read and agreed to the published version of the manuscript.

Funding: This research was co-funded by the European Regional Development Fund of the European Union and Greek national funds through the Operational Program Competitiveness, Entrepreneurship and Innovation, under the call RESEARCH—CREATE—INNOVATE (project code: T2EDK-00362).

Data Availability Statement: Data presented in this study are available upon request from the corresponding author.

Conflicts of Interest: The authors declare no conflict of interest.

References

1. Boltz, J.; Boltz, J.P.; Smets, B.F.; Rittmann, B.E.; Loosdrecht, M.C.M. Van; Morgenroth, E.; Daigger, G.T. From biofilm ecology to reactors : A focused review From bio fi lm ecology to reactors : a focused review. **2017**.
2. Saidulu, D.; Majumder, A.; Gupta, A.K. A systematic review of moving bed biofilm reactor, membrane bioreactor, and moving bed membrane bioreactor for wastewater treatment: Comparison of research trends, removal mechanisms, and performance. *Journal of Environmental Chemical Engineering* **2021**, *9*, 106112.
3. Leyva-Díaz, J.C.; Monteoliva-García, A.; Martín-Pascual, J.; Munio, M.M.; García-Mesa, J.J.; Poyatos, J.M. Moving bed biofilm reactor as an alternative wastewater treatment process for nutrient removal and recovery in the circular economy model. *Bioresource Technology* **2020**, *299*, 122631.
4. Liu, J.; Sun, F.; Zhang, P.; Zhou, Y. Integrated powdered activated carbon and quorum quenching strategy for biofouling control in industrial wastewater membrane bioreactor. *Journal of Cleaner Production* **2021**, *279*, 123551.
5. Banti, D.C.; Tsangas, M.; Samaras, P.; Zorpas, A. LCA of a membrane bioreactor compared to activated sludge system for municipal wastewater treatment. *Membranes* **2020**, *10*, 1–15.
6. Lemonidis, I.; Banti, D.C.; Tzenos, C.A.; Kalamaras, S.D.; Kotsopoulos, T.A.; Samaras, P. Energy Valorization of Fine Screenings from a Municipal Wastewater Treatment Plant. *Energies* **2022**, *15*.
7. Kawan, J.A.; Abu Hasan, H.; Suja, F.; Jaafar, O.; Abd-Rahman, R. A review on sewage treatment and polishing using moving bed bioreactor (Mbbr). *Journal of Engineering Science and Technology* **2016**, *11*, 1098–1120.
8. Banti, D.C.; Samaras, P.; Tsioptsias, C.; Zouboulis, A.; Mitrakas, M. Mechanism of SMP aggregation within the pores of hydrophilic and hydrophobic MBR membranes and aggregates detachment. *Separation and Purification Technology* **2018**.
9. Banti, D.C.; Karayannakidis, P.D.; Samaras, P.; Mitrakas, M.G. An innovative bioreactor set-up that reduces membrane fouling by adjusting the filamentous bacterial population. *Journal of Membrane Science* **2017**.
10. Kampouris, I.D.; Karayannakidis, P.D.; Banti, D.C.; Sakoula, D.; Konstantinidis, D.; Yiangou, M.; Samaras, P.E. Evaluation of a novel quorum quenching strain for MBR biofouling mitigation. *Water Research* **2018**, *143*, 56–65.

11. Gkotsis, P.; Banti, D.; Pritsa, A.; Mitrakas, M.; Samaras, P.; Peleka, E.; Zouboulis, A. Effect of operating conditions on membrane fouling in pilot-scale mbrs; filaments growth, diminishing dissolved oxygen and recirculation rate of the activated sludge. *Membranes* **2021**, *11*, 1–16.
12. Lin, H.; Zhang, M.; Wang, F.; Meng, F.; Liao, B.Q.; Hong, H.; Chen, J.; Gao, W. A critical review of extracellular polymeric substances (EPSs) in membrane bioreactors: Characteristics, roles in membrane fouling and control strategies. *Journal of Membrane Science* **2014**, *460*, 110–125.
13. Banti, D.; Mitrakas, M.; Fytianos, G.; Tsali, A.; Samaras, P. Combined effect of colloids and SMP on membrane fouling in MBRs. *Membranes* **2020**, *10*, 1–15.
14. Mcquarriev, J.P.; Boltz, J.P. Moving Bed Biofilm Reactor Technology ; Process Applications , Design , and Performance. **2010**.
15. Dong, Y.; Fan, S.Q.; Shen, Y.; Yang, J.X.; Yan, P.; Chen, Y.P.; Li, J.; Guo, J.S.; Duan, X.M.; Fang, F.; et al. A Novel Bio-carrier Fabricated Using 3D Printing Technique for Wastewater Treatment. *Scientific Reports* **2015**, *5*.
16. Tang, B.; Song, H.; Bin, L.; Huang, S.; Zhang, W.; Fu, F.; Zhao, Y.; Chen, Q. Bioresource Technology Determination of the profile of DO and its mass transferring coefficient in a biofilm reactor packed with semi-suspended bio-carriers. *Bioresource Technology* **2017**, *241*, 54–62.
17. Lee, S.; Badoux, G.O.; Wu, B.; Chong, T.H. Enhancing performance of biocarriers facilitated gravity-driven membrane (GDM) reactor for decentralized wastewater treatment: Effect of internal recirculation and membrane packing density. *Science of the Total Environment* **2021**, *762*, 144104.
18. Sun, H.; Liu, H.; Zhang, M.; Liu, Y. A novel single-stage ceramic membrane moving bed biofilm reactor coupled with reverse osmosis for reclamation of municipal wastewater to NEWater-like product water. *Chemosphere* **2021**, *268*, 128836.
19. Barwal, A.; Chaudhary, R. To study the performance of biocarriers in moving bed biofilm reactor (MBBR) technology and kinetics of biofilm for retrofitting the existing aerobic treatment systems : a review. **2014**, 285–299.
20. Felföldi, T.; Jurecska, L.; Vajna, B.; Barkács, K.; Makk, J.; Cebe, G.; Szabó, A.; Záray, G.; Márialigeti, K. Texture and type of polymer fiber carrier determine bacterial colonization and biofilm properties in wastewater treatment. **2015**, *264*, 824–834.
21. Elliott, O.; Gray, S.; Mcclay, M.; Nassief, B.; Nunnelley, A.; Ekong, J.; Kardel, K.; Khoshkhoo, A.; Proaño, G.; David, M.; et al. Design and Manufacturing of High Surface Area 3D-Printed Media for Moving Bed Bioreactors for Wastewater Treatment. **2017**, 144–156.
22. Zhang, Y.; Hsu, H.H.; Wheeler, J.J.; Tang, S.; Jiang, X. Emerging investigator series: Emerging biotechnologies in wastewater treatment: From biomolecular engineering to multiscale integration. *Environmental Science: Water Research and Technology* **2020**, *6*, 1967–1985.
23. Tang, B.; Zhao, Y.; Bin, L.; Huang, S.; Fu, F. Bioresource Technology Variation of the characteristics of bio fi lm on the semi-suspended bio-carrier produced by a 3D printing technique : Investigation of a whole growing cycle. *Bioresource Technology* **2017**, *244*, 40–47.
24. Chioti, A.G.; Tsioni, V.; Patsatzis, S.; Filidou, E.; Banti, D.; Samaras, P.; Economou, E.A.; Kostopoulou, E.; Sfetsas, T. Characterization of Biofilm Microbiome Formation Developed on Novel 3D-Printed Zeolite Biocarriers during Aerobic and Anaerobic Digestion Processes. **2022**.
25. APHA (American Public Health Association) *Standard Methods for the Examination of Water and Wastewater*; Washington, DC, 1998;
26. Hwang, B.K.; Kim, J.H.; Ahn, C.H.; Lee, C.H.; Song, J.Y.; Ra, Y.H. Effect of disintegrated sludge recycling on membrane permeability in a membrane bioreactor combined with a turbulent jet flow ozone contactor. *Water Research* **2010**, *44*, 1833–1840.
27. Hartree, E.F. Determination of protein: A modification of the Lowry method that gives a lineart photometric response. *Analytical Biochemistry* **1972**, *48*.
28. Dubois, M.; Gilles, K.A.; Hamilton, J.K.; Rebers, P.A.; Smith, F. Colorimetric Method for Determination of Sugars and Related Substances. **1956**, 350–356.
29. Eikelboom, D.H. *Process control of activated sludge plants by microscopic investigation*; IWA Publishing: Zutphen, 2000;
30. Banti, D.C.; Mitrakas, M.; Samaras, P. Membrane fouling controlled by adjustment of biological treatment parameters in step-aerating MBR. *Membranes* **2021**, *11*, 1–15.
31. Bolyen, E.; Rideout, J.R.; Dillon, M.R.; Bokulich, N.A.; Abnet, C.C.; Al-Ghalith, G.A.; Alexander, H.; Alm, E.J.; Arumugam, M.; Asnicar, F.; et al. Reproducible, interactive, scalable and extensible microbiome data science using QIIME 2. *Nature Biotechnology* **2019**, *37*, 852–857.
32. Benjamin, C.; McMurdie, P.; Rosen, M.; Han, A.; Johnson, A.; Holmes, S. DADA2:High resolution sample inference from Illumina amplicon data. *Encyclopedia of Medical Immunology* **2020**, *13*, 1–7.
33. Quast, C.; Pruesse, E.; Yilmaz, P.; Gerken, J.; Schweer, T.; Yarza, P.; Peplies, J.; Glöckner, F.O. The SILVA ribosomal RNA gene database project: Improved data processing and web-based tools. *Nucleic Acids Research* **2013**, *41*, 590–596.

34. Borea, L.; Naddeo, V.; Belgiorno, V. *Frontiers in wastewater treatment and modelling-An electro moving bed membrane bioreactore (eMB-MBR) as a novel technology for wastewater treatment and reuse*; Mannina, G., Ed.; Springer Netherlands, 2017; ISBN 9783319584201.
35. Abdelfattah, A.; Hossain, M.I.; Cheng, L. High-strength wastewater treatment using microbial biofilm reactor: a critical review. *World Journal of Microbiology and Biotechnology* **2020**, *36*.
36. Shreve, M.J.; Brennan, R.A. Trace organic contaminant removal in six full-scale integrated fixed-film activated sludge (IFAS) systems treating municipal wastewater. *Water Research* **2019**, *151*, 318–331.
37. Mazioti, A.A.; Koutsokeras, L.E.; Constantinides, G.; Vyrides, I. Untapped potential of moving bed biofilm reactors with different biocarrier types for bilge water treatment: A laboratory-scale study. *Water (Switzerland)* **2021**, *13*.
38. Zhou, Y.; Kiely, P.D.; Kibbee, R.; Ormeci, B. Effect of polymeric support material on biofilm development, bacterial population, and wastewater treatment performance in anaerobic fixed-film systems. *Chemosphere* **2021**, *264*, 128477.
39. Qin, S.; Wainaina, S.; Liu, H.; Soufiani, A.M.; Pandey, A.; Zhang, Z.; Awasthi, M.K.; Taherzadeh, M.J. Microbial dynamics during anaerobic digestion of sewage sludge combined with food waste at high organic loading rates in immersed membrane bioreactors. *Fuel* **2021**, *303*, 121276.
40. Gerber, E.; Bernard, R.; Castang, S.; Chabot, N.; Coze, F.; Dreux-Zigha, A.; Hauser, E.; Hivin, P.; Joseph, P.; Lazarelli, C.; et al. Deinococcus as new chassis for industrial biotechnology: Biology, physiology and tools. *Journal of Applied Microbiology* **2015**, *119*, 1–10.
41. Gielnik, A.; Pechaud, Y.; Huguenot, D.; Esposito, G.; Guibaud, G.; van Hullebusch, E.D. *Potential Use of Waste-to-Bioenergy By-Products in Bioremediation of Total Petroleum Hydrocarbons (TPH)-Contaminated Soils*; 2020; ISBN 9783030403485.
42. Tong, J.; Cui, L.; Wang, D.; Wang, X.; Liu, Z. Assessing the performance and microbial structure of biofilms in membrane aerated biofilm reactor for high p-nitrophenol concentration treatment. *Journal of Environmental Chemical Engineering* **2022**, *10*, 108635.
43. Wang, X.; Gao, C.; Jin, P.; Zhang, Y.; Xie, Y.; Chen, T.; Zhang, A. Nitrogen removal performance and bacterial community in a full-scale modified Orbal oxidation ditch with internal nitrate recycle and biocarriers. *Journal of Water Process Engineering* **2021**, *40*, 101791.
44. Wu, X.; Wang, C.; Wang, D.; Huang, Y.X.; Yuan, S.; Meng, F. Simultaneous methanogenesis and denitrification coupled with nitrifying biofilm for high-strength wastewater treatment: Performance and microbial mechanisms. *Water Research* **2022**, *225*, 119163.